Resonance-induced ionization enhancement and suppression of circular states of the hydrogen atom in strong laser fields

Yong Zhao,[1] Yueming Zhou ⬡,[1,*] Qinghua Ke,[1] Jingtai Liang,[1] Yijie Liao ⬡,[1] Min Li,[1] and Peixiang Lu[1,2,†]

[1]*School of Physics, Huazhong University of Science and Technology, Wuhan 430074, China*
[2]*Hubei Key Laboratory of Optical Information and Pattern Recognition, Wuhan Institute of Technology, Wuhan 430205, China*

We theoretically investigated the ionization dynamics of a hydrogen atom in circular excited states irradiated by the circularly polarized laser pulses by solving the time-dependent Schrödinger equation. We calculated the ionization yields of the two excited states which are corotating and counter-rotating with respect to the laser fields as a function of the laser frequency. For the corotating excited state, our results show an obvious ionization suppression when the laser frequency is beyond the one-photon ionization threshold, and it is followed by a strong ionization enhancement when the laser frequency further increases. These ionization suppressions and enhancements are absent for the counter-rotating excited state. By tracing the ionization process, we found that resonance between the initial state and a lower-energy state occurs at the frequency of the ionization enhancement. Ionization from this lower-energy state is responsible for this ionization enhancement. At the frequency of ionization suppression, Rabi oscillation between the initial and the lower-energy state occurs, which prevents further ionization and thus suppresses the final ionization yield.

I. INTRODUCTION

Tunneling ionization (TI) and multiphoton ionization (MPI) are two primary mechanisms of atomic photoionization in strong laser fields [1]. Usually, the Keldysh parameter [2] $\gamma = \sqrt{I_p/2U_p}$ is used to discriminate among adiabatic tunneling ($\gamma \ll 1$), nonadiabatic tunneling [3] ($\gamma \sim 1$), and multiphoton ionization [4] ($\gamma \gg 1$). Here $U_p = F^2/4\omega^2$ is the ponderomotive energy of the laser, I_p is the ionization potential, ω is the laser frequency, and F is the amplitude of the laser field. In typical experimental conditions, electron tunneling should be understand as a nonadiabatic process, while the key assumptions regarding adiabaticity of optical tunneling may quickly become inaccurate. For a sufficiently intense and low-frequency laser field, the barrier-suppressed ionization (BSI, or above-barrier ionization, OBI) takes place [5]. In BSI, the initial state energy level lies above the effective Coulomb barrier suppressed by the field. An important parameter in BSI is the barrier-suppression field strength (or BSI ionization threshold), which defines the minimum field strength at which BSI ionization can occur. For a hydrogen atom at state $|n\rangle$, the BSI ionization threshold are $F_{BSI} = 1/3n^5$ in the linearly polarized (LP) field and $F_{BSI} = 1/16n^4$ in the circularly polarized (CP) field [6,7].

Recently, much attention has been paid to the selectivity of strong-field ionization on the electron rotation in the CP fields, i.e., the dependence of the ionization process on the sign of the magnetic quantum number m of the atom in CP laser field (m dependence) [8–11]. Previous works have revealed the difference in the ionization process of the "corotating" case and "counter-rotating" case [12,13] (for the same or opposite rotation of the initial current density of the active electron with respected to the laser field). It is well known that in the case of single-photon ionization, the corotating state is depleted more efficiently than the counter-rotating sate [14]. It is the same for the ionization of circular Rydberg states in circularly polarized microwave fields. Ionization is much more likely for the Rydberg electron corotating with the field, preferably with the same angular velocity [15,16]. However, the situation is the reverse in the nonadiabatic tunneling regime. Optical tunneling selectively depletes the counter-rotating initial state [17–19].

The first experimental observation of the dependence of the tunneling ionization rate on the sign of magnetic quantum number m was reported in 2012 [20]. Later, a large number of experimental [9,10,21] and theoretical [22–35] studies on the m dependence of the ionization dynamics were reported. Most of the above works are devoted to the m dependence in adiabatic or nonadiabatic tunneling regimes. In the MPI region, it has been shown that the ratio of ionization probabilities for corotating state to counter-rotating state exhibits a strong dependence on the intensity of the laser field [9,11,25–27,36]. The Freeman resonances [37], where ionization is enhanced by transient resonance due to ac Stark shifts of intermediate levels [38–45], make the m dependence of the ionization probability complicated. The ionization can be polarization-selective enhanced by resonance in MPI of the excited atom, which makes it possible to control the electron emission and create a spin-polarized electron pulse with a reversible switch on a femtosecond time scale [9,11,46,47].

In this paper we focus on the resonance in few-photon ionization and the sensitivity of m dependence to the frequency

*zhouymhust@hust.edu.cn
†lupeixiang@hust.edu.cn

change of the ionizing radiation. We theoretically investigated the ionization dynamics of hydrogen atoms in circular states irradiated by the circularly polarized laser pulses by solving the time-dependent Schrödinger equation. Circular states of an atom are excited states with the biggest absolute value of the magnetic quantum number m of the bound state. For a given n there are always two circular states, namely, $(n, l = n - 1, m = n - 1)$ and $(n, l = n - 1, m = -[n - 1])$. We calculated the ionization yields of the two circular states corotating [H(3,2,2)] and counter-rotating [H(3,2,-2)] as a function of the laser frequency. For the corotating excited state, our results show an obvious ionization suppression when the laser frequency is beyond the one-photon ionization threshold, and it is followed by a strong ionization enhancement when the laser frequency further increases. This ionization suppression and enhancement is absent for the counter-rotating excited state. By tracing the time evolution of the magnetic quantum number m, we found that resonance between the initial state and a lower-energy state occurs at the frequency of ionization enhancement. Ionization from this lower-energy state is responsible for this ionization enhancement. At the frequency of ionization suppression, Rabi oscillation between the initial and lower-energy state occurs, which prevents further ionization. The results of different pulse duration are also shown in this paper.

This paper is organized as follows. In Sec. II we briefly summarize the methods used to solve the time-dependent Schrödinger equation for the interaction of the hydrogen atom with a CP laser pulse. The results of the numerical calculations are then presented and analyzed in Sec. III. The conclusions are given in Sec. IV.

Unless specified otherwise, atomic units (a.u.) are used throughout this paper.

II. THEORETICAL MODEL

In this paper we study the ionization dynamics of excited hydrogen atoms by numerically solving the three-dimensional time-dependent Schrödinger equation ((3) D-TDSE). The Schrödinger equation is

$$i \frac{\partial \psi(\mathbf{r}, t)}{\partial t} = H(\mathbf{r}, t) \psi(\mathbf{r}, t), \tag{1}$$

where

$$H(\mathbf{r}, t) = -\frac{1}{2} \nabla^2 - \frac{1}{r} - i\mathbf{A}(t) \cdot \nabla. \tag{2}$$

We consider a hydrogen atom under an anticlockwise CP pulse in the x-y plane with vector potential

$$\mathbf{A}(t) = A_0 f(t)[-\mathbf{x} \sin(\omega t) + \mathbf{y} \cos(\omega t)], \tag{3}$$

where $A_0 = F_0/\omega$ is the amplitude of the vector potential, and $f(t)$ is a slowly varying pulse envelope which has a sine-squared form,

$$f(t) = \sin^2\left(\frac{\pi t}{\tau}\right), \tag{4}$$

where $\tau = NT$ is the total pulse duration and T is the pulse period. The 3D-TDSE in Eq. (1) is solved in the spherical coordinate where the wave function $\psi(\mathbf{r}, t)$ is expanded by

spherical harmonics $|l, m\rangle$:

$$|\psi(\mathbf{r}, t)\rangle = \sum_{l,m} \frac{R_{lm}(r, t)}{r} |l, m\rangle. \tag{5}$$

Here $R_{lm}(r, t)$ is the radial part of the wave function, which is discretized by a finite-element discrete variable representation method [48]. The time propagation of the TDSE is calculated by the split-Lanczos method [49,50].

The larger spatial extension of the Rydberg states requires large radial boxes when propagated in time. In our computations we use boxes with an upper bound of 900 a.u. and the angular basis is $l_{\max} = 30$. The convergence of our calculations has been confirmed by enlarging the box size and $l_{\max}$.

The population of the excited state is gain by projecting the wave function onto hydrogen bound states,

$$P_{\mathrm{nlm}} = |\langle \psi_{\mathrm{nlm}} | \psi(\mathbf{r}, T)\rangle|^2, \tag{6}$$

and the ionization probability is obtained from

$$P_{\mathrm{ion}} = 1 - \sum_{n=1}^{31} \sum_{l=0}^{30} \sum_{m=-30}^{30} |\langle \psi_{\mathrm{nlm}} | \psi(\mathbf{r}, T)\rangle|^2. \tag{7}$$

The ionization yield has also been calculated by projecting the final wave function onto the continuum state function (the Coulomb wave function). The obtained results are the same as those from Eq. (7), confirming the validity of our calculations.

III. RESULTS AND DISCUSSION

A. Numerical results

Figure 1 displays the ionization probabilities of the excited state of the hydrogen atom in the CP laser field as a function of laser frequency. Here we calculated the ionization probabilities for two excited states of H. The blue curve in Fig. 1(a) represents the initial state $(n, l, m) = (3,2,2)$, which is corotating with respect to the laser field. The red dotted curve in Fig. 1(a) represents the initial state $(3,2,-2)$, which is counter-rotating with the laser field. The intensity of the laser pulse is 8×10^{12} W/cm^2. Two pulse durations have been considered here. Figures 1(a) and 1(b) display the results for $\tau = 8$ and 30 T, respectively.

It can been seen in Fig. 1(a) that at low laser frequencies the ionization probabilities for both states are approximately 100%. This is because the dominant ionization mechanism is barrier-suppression ionization (BSI). At the low frequencies the laser field could be treated as the quasistatic field. For the CP laser field, the ionization threshold of BSI for the state $n = 3$ is about $F_{\mathrm{BSI}} = 1/16n^4 = 0.000\,77$ a.u. [6]. The electric field of our laser pulses is $F = 0.0151$ a.u., larger than F_{BSI}. Thus the BSI dominates and the ionization probabilities approach 100%. As the laser frequency increases, the ionization probabilities decrease. Interestingly, the ionization probability of the state counter-rotating with the laser field is higher than that of the corotating state. This behavior could be understood as the nonadiabatic effect in strong-field ionization. Previous studies have shown that in the tunneling ionization region, the state counter-rotating with the laser field has higher ionization probability than that of the corotating state due to the nonadiabatic effect [17–19]. This is responsible for the
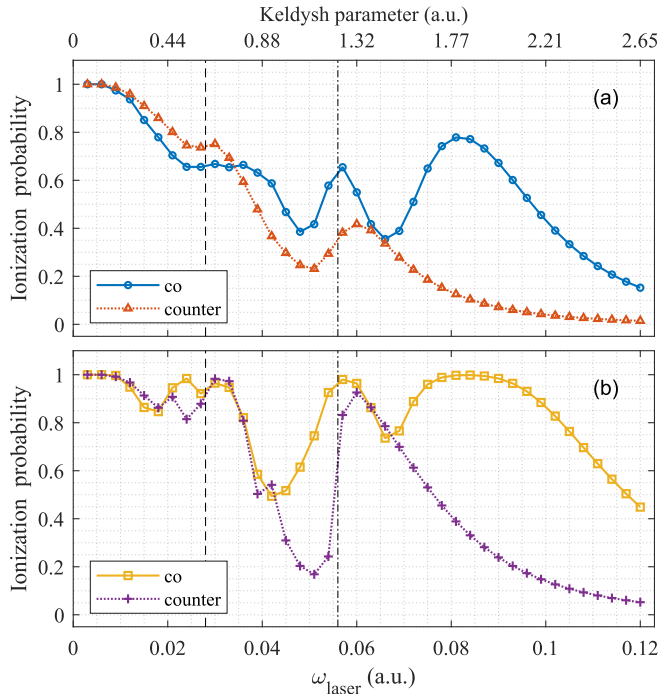
FIG. 1. The ionization probabilities of two initial states of hydrogen atoms as a function of the laser frequency. The upper axis represents the Keldysh parameters, corresponding to the laser frequencies. In the legend "Co" indicates the initial state $(n, l, m) = (3,2,2)$ corotating with respect to the laser field, and "Counter" represents the initial state $(3,2,-2)$ counter-rotating with respect to the laser field. The vertical dashed and dashed-dotted lines indicate the two- and one-photon ionization thresholds, respectively. The laser intensity is 8×10^{12} W/cm². The pulse durations are (a) $\tau = 8$ T and (b) $\tau = 30$ T.
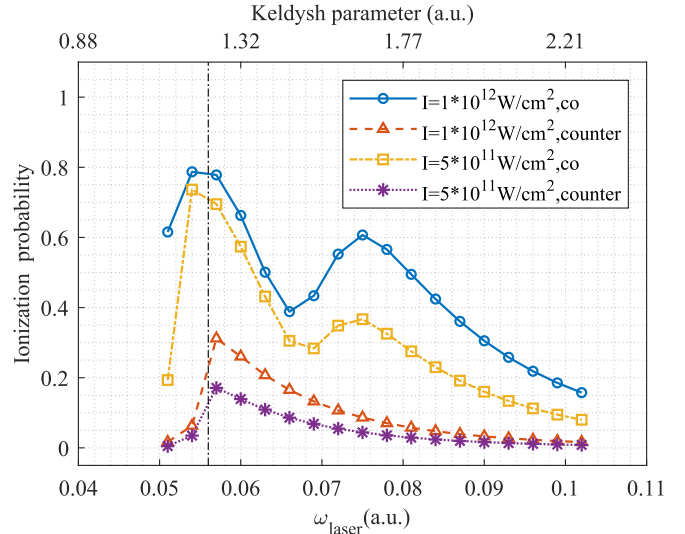

FIG. 2. The ionization probabilities of two initial states of hydrogen atoms as a function of the laser frequency. In the legend "Co" indicates the initial state $(n, l, m) = (3,2,2)$ corotating with respect to the laser field, and "Counter" represents the initial state $(3,2,-2)$ counter-rotating with respect to the laser field. The vertical dashed-dotted line indicates the one-photon ionization threshold. The laser intensities are 1×10^{12} W/cm² for the cycles and triangles and 5×10^{11} W/cm² for the squares and asterisks, respectively. The pulse duration is $\tau = 30$ T.

higher ionization probability of the counter-rotating state in our calculations.

As the laser frequency further increases, multiphoton ionization becomes the dominant mechanism. The dashed lines in Fig. 1 indicate the two- and one-photon ionization thresholds, respectively. As expected, a peak appears when the laser frequency increases through the two-photon and one-photon ionization thresholds [45]. Different from the lower-frequency region, here the ionization probability of the corotating state is higher than that of the counter-rotating state [9,11,27]. At the frequencies much higher than the one-photon ionization threshold, the ionization probability of the corotating state is higher than that of the counter-rotating state. This behavior has been well demonstrated in textbooks that state single-photon ionization prefers corotating electrons [14].

The most interesting characteristics appear at frequencies $\omega_{laser} \sim 0.06$ a.u. $- 0.09$ a.u. In this region, the ionization probability of the counter-rotating state decreases monotonously. However, for the corotating state, there is an obvious dip at around ω_{laser}=0.066 a.u. and a giant peak near ω_{laser}=0.081 a.u. These phenomena exist for both pulse durations, as shown in Figs. 1(a) and 1(b). For both states, the overall features are the same for the two pulse durations. The dip at ω_{laser}=0.066 a.u. and the giant peak at ω_{laser}=0.081 a.u. for the corotating state are similar for the two pulse durations. These character-

istics are the main focus of this paper, and we will reveal the underlying dynamics.

Figure 2 shows the results of two initial states with two different laser intensities. The laser intensity are 1×10^{12} W/cm² for the cycles and the triangles and 5×10^{11} W/cm² for the squares and the asterisks, respectively. The pulse duration is $\tau = 30$ T. For both laser intensities, the overall features are the same.

B. The ionization pathways of the circular excited states

In order to understand the difference in ionization probability between the co- and counter-rotation states, we analyze the excitation pathways of the two circular excited states. The dipole selection rules for the circular states in the CP field are

$$\text{Corotating state } (3,2,2): \Delta m = +1, \Delta l = +1$$

$$\text{Counter-rotating state } (3,2,-2): \Delta m = +1, \Delta l = \pm 1 \quad (8)$$

for absorbing one photon and

$$\text{Corotating state } (3,2,2): \Delta m = -1, \Delta l = -1$$

$$\text{Counter-rotating state } (3,2,-2): \Delta m = -1, \Delta l = \pm 1 \quad (9)$$

for emitting one photon, respectively.

Figure 3 shows the diagram of excitation pathways of the two initial states according to the dipole selection rules in lowest-order perturbation theory (LOPT) [4]. Figure 3(a) shows the pathways of the corotating state $(n, l, m) = (3, 2, 2)$, and Fig. 3(b) shows the pathways of the counter-rotating state $(3,2,-2)$. The yellow (light gray) rectangle represents the initial state, and the green (dark gray) rectangle represents the excited states which are allowed by
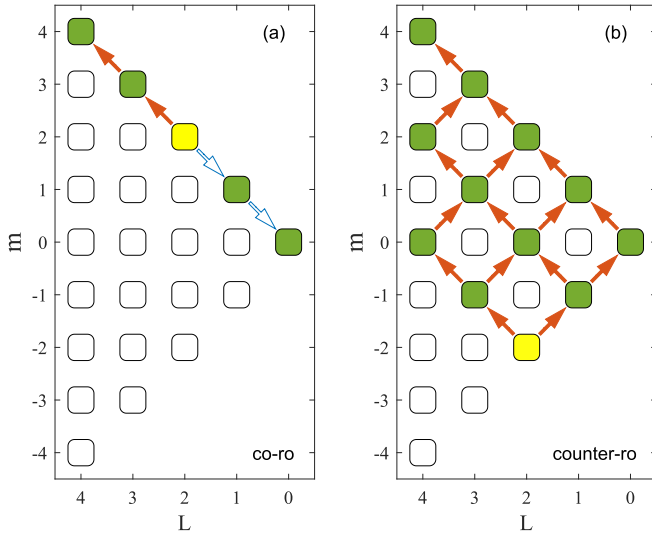
FIG. 3. The diagram of excitation pathways according to the dipole selection rules in lowest-order perturbation theory for (a) the corotating initial state $(n, l, m) = (3, 2, 2)$ and (b) the counter-rotating state (3,2,-2). The horizontal axis represents the angular quantum number L, and the vertical axis represents the magnetic quantum number m. The yellow (light gray) rectangle represents the initial state, and the green (dark gray) rectangle represents the excited states which are allowed by the dipole selection rules. The red (dark gray) arrow represents absorbing one photon and the blue hollow arrow represents emitting one photon.

FIG. 4. The distribution of (l, m) states obtained by summing over n by solving the 3D-TDSE for (a) corotating initial state $(n, l, m) = (3, 2, 2)$ and (b) counter-rotating initial state (3,2,-2) at the end of the laser pulse. The black asterisks mark the initial states. The horizontal axis represents the angular quantum number L and the vertical axis represents the magnetic quantum number m. The laser frequency, laser intensity, and pulse duration are $\omega = 0.027$ a.u., $I = 8 \times 10^{12}$ W/cm^2 and $\tau = 8$ T, respectively.

the dipole selection rules. The red (dark gray) arrow represents absorbing one photon, and the blue hollow arrow represents emitting one photon. For the corotating state in Fig. 3(a), the initial circular state can be excited into higher-energy states or decay into lower-energy states which satisfy the equation $l = m$, as shown in Fig. 3(a).

For the counter-rotating state in Fig. 3(b), there are multiple excitation pathways, and the initial state can be exited into a series of higher-energy states through the crossed pathways. The biggest difference of the counter-rotating state is that there is no pathway for the initial state to decay into a lower-energy state by emitting photons, which is allowed in the corotating case. Indeed, the lower-energy state plays a very important role in the ionization process, as will be shown below.

Figure 4 shows the (l, m) state distributions for the two initial states obtained by summing over n by solving 3D-TDSE at the end of the laser pulse. Figure 4(a) shows the result of corotating initial state $(n, l, m) = (3, 2, 2)$, and Fig. 4(b) shows the result of a counter-rotating initial state (3,2,-2). The black asterisks mark the initial states. Here the laser frequency, laser intensity, and pulse duration are $\omega = 0.027$ a.u., $I = 8 \times 10^{12}$ W/cm^2, and $\tau = 8$ T, respectively.

It can be seen in Fig. 4(a) that the electrons are mainly distributed in a series of (l, m) states which satisfy the equation $l = m$ for the corotating initial state. Figure 4(b) shows a checkerboard distribution that the counter-rotating initial state has been excited to a series of higher-energy states, while there is no population in the lower-energy state. Obviously, the (l, m) state distributions of the TDSE results in Fig. 4 are
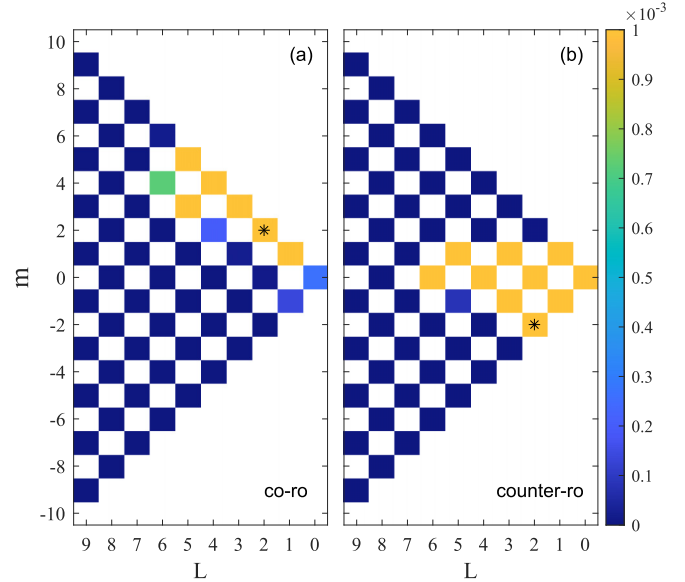
in good agreement with the excitation pathways analysis in Fig. 3.

The distribution of the neighbor state beside the excitation pathways indicated in Fig. 3 comes from the channel that ignored the approximation of LOPT [4], where the electron first jumps to a excited state (with a large principal quantum number n) and then decays into that neighbor state by emitting one photon. For example, the distribution in the (5,3) state of Fig. 4(a) can be populated by emitting one photon from the (4,4) state $[(l, m) = (4, 4) \rightarrow (5, 3)]$. Similarly, the distribution in the (6,0) state in Fig. 4(b) can be populated by emitting one photon from the (5,1) state $[(l, m)=(5, 1) \rightarrow (6, 0)]$. The blank cells in Fig. 4 represent the states which are forbidden by the dipole selection rules.

C. Resonance-induced ionization enhancement

In the CP field, the electron absorbs one photon, increasing the magnetic number by $\Delta m = +1$, and emits one photon, decreasing the magnetic number by $\Delta m = -1$. The changing of the magnetic quantum number m reflects the photon absorption in the ionization process. In order to reveal the underlying dynamic of the giant peak near $\omega_{laser} = 0.081$ a.u. in Fig. 1, we trace the time evolution of the magnetic quantum number m by solving the 3D-TDSE, as shown in Fig. 5. Figures 5(a) and 5(b) show the results of the corotating initial state $(n, l, m) = (3, 2, 2)$ and counter-rotating initial state (3,2,-2), respectively. Here the laser frequency, laser intensity, and pulse duration are $\omega = 0.081$ a.u., $I = 8 \times 10^{12}$ W/cm^2, and $\tau = 8$ T, respectively. The red (dark gray) arrow represents absorbing one photon, and the blue hollow arrow
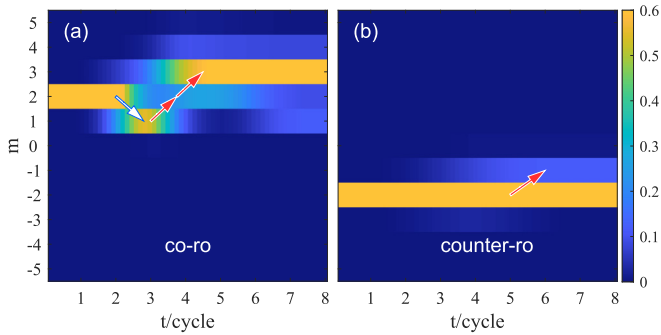
FIG. 5. The m distributions as a function of time by solving 3D-TDSE for (a) the corotating initial state $(n, l, m) = (3,2,2)$ and (b) the counter-rotating initial state $(3,2,-2)$. The laser intensity is 8×10^{12} W/cm^2, the pulse duration is $\tau = 8$ T, and the laser frequency is $\omega = 0.081$ a.u. The red (dark gray) arrow represents absorbing one photon, and the blue hollow arrow represents emitting one photon.

represents emitting one photon. Note that the frequency of the giant peak locates in the single-photon ionization region. Therefore, for the corotating initial state [Fig. 5(a)], the states with $m = 3$ represent the continuum state. The states with $m = 1$ represent the lower-energy bound state. Similarly, for the counter-rotating initial state [Fig. 5(b)], the states $m = -3$ and $m = -1$ represent the lower-energy bound states and the continuum state, respectively. For the counter-rotating state in Fig. 5(b), there is only one ionization channel where the electron is ionized directly to the continuum state by absorbing one photon.

For the corotating state in Fig. 5(a), there are two ionization channels. One is where the electron is ionized directly by absorbing one photon, and the other one is that the electron decays into a lower-energy state, first by emitting one photon and then being ionized to the continuum state by absorbing two photons. Figure 5(a) shows that the second ionization channel dominates. The final ionization probability of the corotating state is much greater than that of the counter-rotating state. In other words, the ionization is enhanced by resonance with the lower-energy state. This indicates that electrons are more likely to be ionized when they decay into the lower-energy state where the electron is closer to the nucleus. Previous studies have demonstrated that electrons have the largest ionization probability at their nearest point to the nucleus [24,51,52]. The Coulomb force interaction with the nucleus is the catalyst for ionization.

In summary, at the frequency of the giant peak of the corotating initial state, the ionization is enhanced by resonance with the lower-energy state, which is forbidden by the dipole selection rules for the counter-rotating circular state.

D. Resonance-induced ionization suppression

In strong laser fields, resonance occurs in a wide range of laser frequency because of the wide frequency spectrum of the pulse and the ac Stark shift of the energy levels [38–45]. For the H atom, the field-free energy difference between state $n = 3$ and $n = 2$ is 0.07 a.u. However, a dip appears at $\omega_{laser} = 0.07$ a.u. The analyses above show that resonance is responsible for the giant peak of the ionization probability at
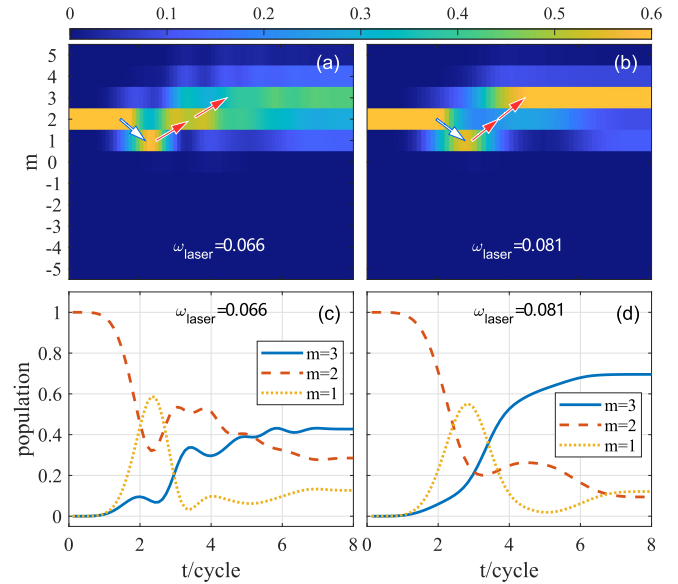

FIG. 6. The distribution of m states as a function of time for the corotating initial state $(3,2,2)$ and different laser frequencies for (a), (c) 0.066 a.u. and (b), (d) 0.081 a.u. Here the laser intensities are 8×10^{12} W/cm^2 and the pulse durations are $\tau = 8$ T. The red (dark gray) arrow represents absorbing one photon, and the blue hollow arrow represents emitting one photon.

$\omega = 0.081$ a.u. At the frequency $\omega = 0.07$ a.u., instead of the ionization enhancement there is a surprising dip in Fig. 1(a) for the corotating state, i.e., resonance induces the ionization suppression. This is different from previous studies in the MPI region, where resonance always enhances the ionization yield [9,11,45].

In order to reveal the underlying dynamics of ionization suppression, we trace the time evolution of the magnetic quantum number m at the frequency of the ionization suppression ($\omega_{laser} = 0.066$ a.u.) in the 3D-TDSE calculation, as shown in Fig. 6(a). It is more clearly seen in Fig. 6(c), where we replotted the curves of three m state populations ($m = 1, 2, 3$) as a function of time using the data of Fig. 6(a). To compare with the results at the frequency of ionization enhancement ($\omega_{laser} = 0.081$ a.u.), we replotted the data of Fig. 5(a) in Fig. 6(b) and the curves of three m states in Fig. 6(d). The red (dark gray) arrow represents absorbing one photon and the blue hollow arrow represents emitting one photon. Note that both the laser frequencies we show are located in the single-photon ionization region. Therefore the states $m = 1$, $m = 2$, and $m = 3$ in Fig. 6 represent the lower-energy state, initial state, and continuum state, respectively. We focus on the population of these three m states.

At the frequency of ionization enhancement in Fig. 6(d), the population of the initial state ($m = 2$) decreases sharply at the beginning of the laser pulse. Most of them decay into the lower-energy state ($m = 1$), corresponding to the rapid rise of the yellow dotted curve, while only a few electrons are ionized directly into the continuum state ($m = 3$). As the time increases, the yellow dotted curve decreases sharply after a peak, while the blue curve increases sharply. This indicates that most of the electrons in $m = 1$ state are ionized directly
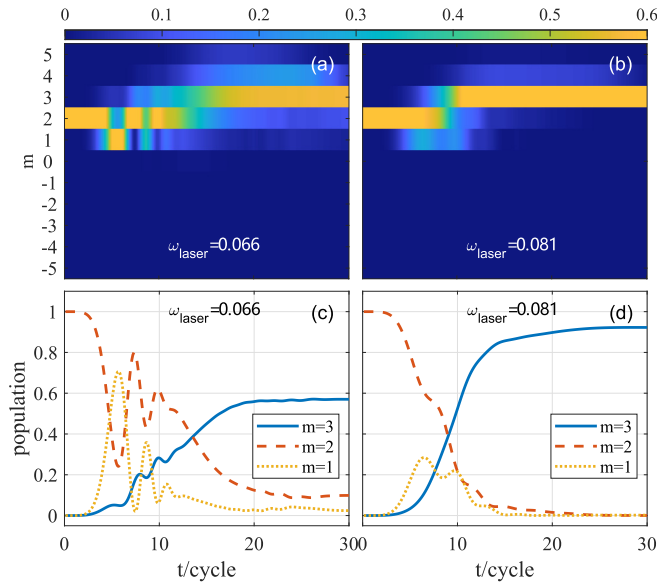
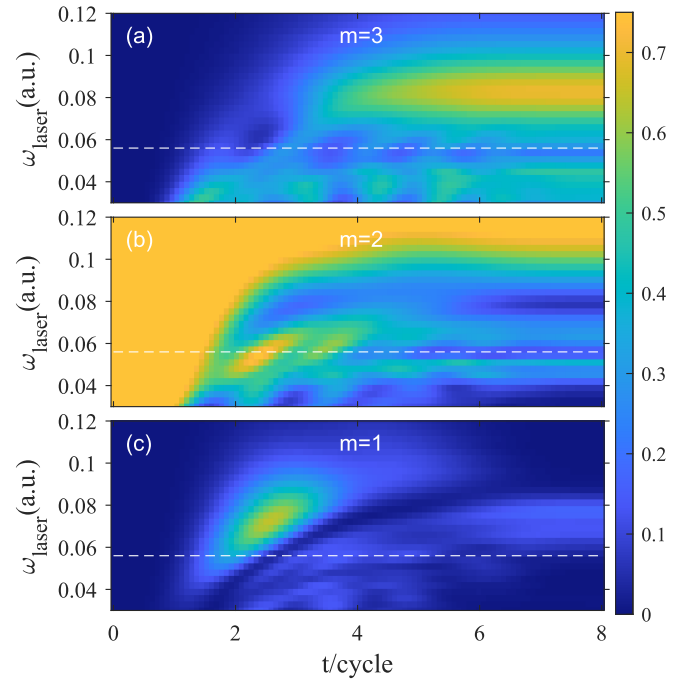FIG. 7. The same as those in Fig. 6 but for pulse duration $\tau = 30$ T.

FIG. 8. The distribution of (a) $m = 3$, (b) $m = 2$, and (c) $m = 1$ states as a function of time and laser frequency for the corotating initial state H(3,2,2). The white dotted lines represent the single-photon ionization threshold $\omega = 0.056$ a.u. The white ellipse represents the resonance region. The laser intensity is 8×10^{12} W/cm^2, and the pulse duration is $\tau = 8$ T.

to the continuum state ($m = 3$) by absorbing two photons, while only a few electrons return back to the initial state ($m = 1$) by absorbing one photon. At the frequency of ionization suppression in Fig. 6(c), the population of the initial state ($m = 2$) decreases sharply at the beginning of the laser pulse as well. Most of them decay into the lower-energy resonated state ($m = 1$). Different from the results of Fig. 6(d), more electrons return back to the initial state ($m = 2$) in Fig. 6(c). Importantly, an obvious oscillation appears between the populations of the initial state ($m = 2$) and the lower-energy state ($m = 1$). This is the Rabi oscillation between the resonated energy levels [it can be seen more clearly in Fig. 7(c)] [53–56]. At the end of the laser pulse, the population of the $m = 3$ state is smaller than those of Fig. 6(d). More electrons remain in the initial state ($m = 1$). As a result, the final ionization probability of Fig. 6(c) is smaller than that of Fig. 6(d). In other words, the ionization is suppressed by the Rabi oscillation, which is caused by the strong resonance between the initial state and the lower-energy state.

The increase of pulse duration makes the interaction time longer and the frequency spectrum more narrowed. To understand the effects of different pulse durations on resonance, we show the same distribution of m states with pulse duration $\tau = 30$ T in Fig. 7. It can be seen that the overall features in Fig. 7 are same as that in Fig. 6. However, there are two different phenomena. One is that the final ionization probabilities of Fig. 7 are larger than those of Fig. 6 at both frequencies because of the longer interaction time. The other is that the electron which decayed into the lower-energy state ($m = 1$) in Fig. 7(d) is much less than that in Fig. 7(c), and the Rabi oscillation between the initial state ($m = 2$) and the lower-energy state ($m = 1$) is more obvious in Fig. 7(c), which suppresses the ionization. This phenomenon is because the more narrowed frequency spectrum make the resonance detune sharply when the laser frequency is far away from the central resonance frequency $\omega = 0.07$ a.u. These differences

further demonstrate that the ionization is suppressed by the Rabi oscillation, which is caused by the resonance between the initial state and the lower-energy state.

E. Frequency dependence of ionization enhancement and suppression

The resonance occurs in a wide range of laser frequency because of the wide frequency spectrum of the pulse and the ac Stark shift of the energy levels. In order to investigate the frequency dependence of ionization enhancement and suppression of the corotating state, we trace the populations of three m states ($m = 1, 2, 3$) as a function of laser frequency and time, as shown in Fig. 8. Here the laser intensity and pulse duration are 8×10^{12} W/cm^2 and $\tau = 8$ T, respectively. The white dotted lines represent the single-photon ionization threshold 0.056 a.u. When $\omega_{\text{laser}} > 0.056$ a.u., the states $m = 1$, $m = 2$, and $m = 3$ represent the lower-energy resonant state, initial state, and continuum state, respectively. Figure 8(a) shows the distribution of the $m = 3$ state. The maximum at the end of the laser pulse indicates the frequency of ionization enhancement (i.e., the giant peak), which is around $\omega_{\text{laser}} = 0.08$ a.u. Figure 8(c) shows the distribution of the $m = 1$ state. The elliptic area of maximum value indicates the resonance region, where the ionization enhancement and suppression occur. It can be seen that the resonance occurs in a wide range of laser frequency which ranges from 0.06 to 0.09 a.u.

Note that the central frequency of resonance is 0.07 a.u., where the ionization is suppressed due to the Rabi
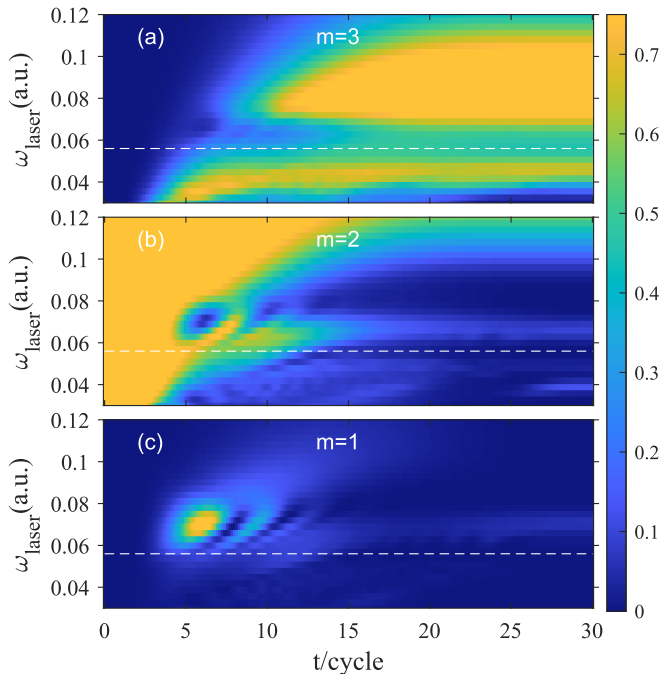
FIG. 9. The same as those in Fig. 8 but for $\tau = 30$ T pulse duration.

oscillation. Figure 8(b) shows the distribution of the $m = 2$ state. Correspondingly, the resonance region reflected in Fig. 8(b) is an elliptic area of minimum value of population.

We show the same distributions of m states with longer pulse durations $\tau = 30$ T in Fig. 9 to compare the effects of two different pulse durations on resonance. It can be seen that the overall features in Fig. 9 are the same as those in Fig. 8. However, there are two different phenomena in Fig. 9(c). First, the resonance region becomes much smaller because of the more narrowed frequency spectrum. Second, it can be seen in Fig. 9(c) that the elliptic resonance region is followed by several circular arcs, which imply the Rabi oscillation between $m = 1$ and $m = 2$ states.

In addition, the corresponding resonance region in Fig. 9(b) is more obvious.

IV. CONCLUSIONS

By solving the three-dimensional time-dependent Schrödinger equation, the ionization dynamics of hydrogen atoms in circular Rydberg states, irradiated by the circularly polarized laser pulses, has been studied. We investigated the ionization yields of the two excited states corotating and counter-rotating with respect to the laser fields as a function of the laser frequency. For the corotating excited state, our results show an obvious ionization suppression when the laser frequency is beyond the one-photon ionization threshold, and it is followed by a strong ionization enhancement when the laser frequency further increases. These ionization suppressions and enhancements are absent for the counter-rotating excited state. By tracing the time evolution of the magnetic quantum number m at the frequency of ionization enhancement and suppression, we found that resonance between the initial state and a lower-energy state is responsible for these phenomena. Ionization from this lower-energy state is responsible for the ionization enhancement. At the frequency of ionization suppression, Rabi oscillation between the initial and the lower-energy state occurs, which prevents further ionization. In addition, we compare the results of two different pulse durations. The Rabi oscillation becomes more obvious at the frequency of resonance for the pulse with longer duration. Our study of resonance between the initial circular Rydberg state and the lower-energy state provides further insight into multiphoton resonant ionization mechanisms.

[1] S. Augst, D. Strickland, D. D. Meyerhofer, S. L. Chin, and J. H. Eberly, Phys. Rev. Lett. **63**, 2212 (1989).

[2] L. V. Keldysh, Sov. Phys. JETP **20**, 1307 (1965).

[3] G. L. Yudin and M. Y. Ivanov, Phys. Rev. A **64**, 013409 (2001).

[4] P. Lambropoulos, Adv. At. Mol. Phys **12**, 87 (1976).

[5] A. Scrinzi, M. Geissler, and T. Brabec, Phys. Rev. Lett. **83**, 706 (1999).

[6] P. Fu, T. J. Scholz, J. M. Hettema, and T. F. Gallagher, Phys. Rev. Lett. **64**, 511 (1990).

[7] T. F. Gallagher, *Rydberg Atoms* (Cambridge University Press, Cambridge, England, 1994).

[8] T. Mazza, M. Ilchen, A. J. Rafipoor, C. Callegari, P. Finetti, O. Plekan, K. C. Prince, R. Richter, M. B. Danailov, A. Demidovich *et al.*, Nat. Commun. **5**, 3648 (2014).

[9] M. Ilchen, N. Douguet, T. Mazza, A. J. Rafipoor, C. Callegari, P. Finetti, O. Plekan, K. C. Prince, A. Demidovich, C. Grazioli, L. Avaldi, P. Bolognesi, M. Coreno, M. DiFraia, M. Devetta,

Y. Ovcharenko, S. Dusterer, K. Ueda, K. Bartschat *et al.*, Phys. Rev. Lett. **118**, 013002 (2017).

[10] S. Eckart, M. Kunitski, M. Richter, A. Hartung, J. Rist, F. Trinter, K. Fehre, N. Schlott, K. Henrichs, L. P. H. Schmidt *et al.*, Nat. Phys. **14**, 701 (2018).

[11] A. H. N. C. De Silva, D. Atri-Schuller, S. Dubey, B. P. Acharya, K. L. Romans, K. Foster, O. Russ, K. Compton, C. Rischbieter, N. Douguet, K. Bartschat, and D. Fischer, Phys. Rev. Lett. **126**, 023201 (2021).

[12] M. Gajda, B. Piraux, and K. Rzacewski, Phys. Rev. A **50**, 2528 (1994).

[13] E. Huens, B. Piraux, A. Bugacov, and M. Gajda, Phys. Rev. A **55**, 2132 (1997).

[14] H. Bethe, *Intermediate Quantum Mechanics* (W. A. Benjamin, New York, 1964).

[15] K. Rzacewski and B. Piraux, Phys. Rev. A **47**, R1612(R) (1993).

[16] J. Zakrzewski, D. Delande, J.-C. Gay, and K. Rzacewski, Phys. Rev. A **47**, R2468(R) (1993).

[17] I. Barth and O. Smirnova, Phys. Rev. A **84**, 063415 (2011).

[18] I. Barth and O. Smirnova, Phys. Rev. A **87**, 013433 (2013).

[19] I. Barth and O. Smirnova, Phys. Rev. A **87**, 065401 (2013).

[20] T. Herath, L. Yan, S. K. Lee, and W. Li, Phys. Rev. Lett. **109**, 043004 (2012).

[21] D. Trabert, A. Hartung, S. Eckart, F. Trinter, A. Kalinin, M. Schöffler, L. P. H. Schmidt, T. Jahnke, M. Kunitski, and R. Dörner, Phys. Rev. Lett. **120**, 043202 (2018).

[22] J. H. Bauer, Phys. Rev. A **84**, 025403 (2011).

[23] J. H. Bauer, J. Phys. B **46**, 045601 (2013).

[24] S. Askeland, S. A. Sørngård, I. Pilskog, R. Nepstad, and M. Førre, Phys. Rev. A **84**, 033423 (2011).

[25] J. H. Bauer, F. Mota-Furtado, P. F. O'Mahony, B. Piraux, and K. Warda, Phys. Rev. A **90**, 063402 (2014).

[26] S.-D. Jheng, T.-F. Jiang, J.-H. Chen, and J.-L. Liu, Phys. Scr. **93**, 085401 (2018).

[27] A. N. Grum-Grzhimailo, N. Douguet, M. Meyer, and K. Bartschat, Phys. Rev. A **100**, 033404 (2019).

[28] G. S. J. Armstrong, D. D. A. Clarke, A. C. Brown, and H. W. van der Hart, Phys. Rev. A **99**, 023429 (2019).

[29] J. H. Bauer, Phys. Rev. A **85**, 063417 (2012).

[30] J. Kaushal and O. Smirnova, Phys. Rev. A **88**, 013421 (2013).

[31] M. Li, L. Qin, C. Wu, L.-Y. Peng, Q. Gong, and Y. Liu, Phys. Rev. A **89**, 013422 (2014).

[32] C. H. Raymond Ooi, W. L. Ho, and A. D. Bandrauk, Phys. Rev. A **90**, 013417 (2014).

[33] C. H. R. Ooi, W. L. Ho, and A. D. Bandrauk, Sci. Rep. **7**, 6739 (2017).

[34] C. A. Mancuso, K. M. Dorney, D. D. Hickstein, J. L. Chaloupka, X.-M. Tong, J. L. Ellis, H. C. Kapteyn, and M. M. Murnane, Phys. Rev. A **96**, 023402 (2017).

[35] D. D. A. Clarke, G. S. J. Armstrong, A. C. Brown, and H. W. van der Hart, Phys. Rev. A **98**, 053442 (2018).

[36] J. H. Bauer and Z. Walczak, Phys. Rev. A **101**, 063409 (2020).

[37] R. R. Freeman, P. H. Bucksbaum, H. Milchberg, S. Darack, D. Schumacher, and M. E. Geusic, Phys. Rev. Lett. **59**, 1092 (1987).

[38] P. Kruit, J. Kimman, H. G. Muller, and M. J. V. der Wiel, J. Phys. B **16**, 937 (1983).

[39] P. Agostini, P. Breger, A. L'Huillier, H. G. Muller, G. Petite, A. Antonetti, and A. Migus, Phys. Rev. Lett. **63**, 2208 (1989).

[40] N. B. Delone and V. P. Krainov, Phys. Usp. **42**, 669 (1999).

[41] R. Wiehle, B. Witzel, H. Helm, and E. Cormier, Phys. Rev. A **67**, 063405 (2003).

[42] M. Li, P. Zhang, S. Luo, Y. Zhou, Q. Zhang, P. Lan, and P. Lu, Phys. Rev. A **92**, 063404 (2015).

[43] N. A. Hart, J. Strohaber, A. A. Kolomenskii, G. G. Paulus, D. Bauer, and H. A. Schuessler, Phys. Rev. A **93**, 063426 (2016).

[44] P. Stammer, S. Patchkovskii, and F. Morales, Phys. Rev. A **101**, 033405 (2020).

[45] D. Chetty, R. D. Glover, B. A. deHarak, X. M. Tong, H. Xu, T. Pauly, N. Smith, K. R. Hamilton, K. Bartschat, J. P. Ziegel, N. Douguet, A. N. Luiten, P. S. Light, I. V. Litvinyuk, and R. T. Sang, Phys. Rev. A **101**, 053402 (2020).

[46] A. H. N. C. De Silva, T. Moon, K. L. Romans, B. P. Acharya, S. Dubey, K. Foster, O. Russ, C. Rischbieter, N. Douguet, K. Bartschat, and D. Fischer, Phys. Rev. A **103**, 053125 (2021).

[47] S. Walker, L. Kolanz, J. Venzke, and A. Becker, Phys. Rev. A **103**, L061101 (2021).

[48] T. N. Rescigno and C. W. McCurdy, Phys. Rev. A **62**, 032706 (2000).

[49] W.-C. Jiang and X.-Q. Tian, Opt. Express **25**, 26832 (2017).

[50] J. Liang, W.-C. Jiang, S. Wang, M. Li, Y. Zhou, and P. Lu, J. Phys. B **53**, 095601 (2020).

[51] A. ten Wolde, L. D. Noordam, A. Lagendijk, and H. B. van Linden van den Heuvell, Phys. Rev. Lett. **61**, 2099 (1988).

[52] B. C. Yang and F. Robicheaux, Phys. Rev. A **90**, 063413 (2014).

[53] I. I. Rabi, Phys. Rev. **49**, 324 (1936).

[54] D. Braak, Phys. Rev. Lett. **107**, 100401 (2011).

[55] T. R. Gentile, B. J. Hughey, D. Kleppner, and T. W. Ducas, Phys. Rev. A **40**, 5103 (1989).

[56] M. Fushitani, C.-N. Liu, A. Matsuda, T. Endo, Y. Toida, M. Nagasono, T. Togashi, M. Yabashi, T. Ishikawa, Y. Hikosaka, T. Morishita, and A. Hishikawa, Nat. Photon. **10**, 102 (2016).